THE JOURNAL OF PHYSICAL CHEMISTRY B

Article

pubs.acs.org/JPCB

Molecular Energetics in the Capsomere of Virus-Like Particle Revealed by Molecular Dynamics Simulations

Lin Zhang,[†] Ronghong Tang,[†] Shu Bai,[†] Natalie K. Connors,[‡] Linda H. L. Lua,[§] Yap P. Chuan,[‡] Anton P. J. Middelberg,[‡] and Yan Sun*,[†]

[†]Department of Biochemical Engineering and Key Laboratory of Systems Bioengineering of the Ministry of Education, School of Chemical Engineering and Technology, Tianjin University, Tianjin 300072, China

[‡]Australian Institute for Bioengineering and Nanotechnology, Centre for Biomolecular Engineering, The University of Queensland, St Lucia, QLD, 4072, Australia

[§]Protein Expression Facility, The University of Queensland, St Lucia, QLD, 4072, Australia

Supporting Information

ABSTRACT: Virus-like particles (VLPs) are highly organized nanoparticles that have great potential in vaccinology, gene therapy, drug delivery, and materials science. However, the application of VLPs is hindered by obstacles in their design and production due to low efficiency of self-assembly. In the present study, all-atom (AA) molecular dynamics (MD) simulations coupled with the molecular mechanics-Poisson–Boltzmann surface area (MM-PBSA) method are utilized to examine the molecular interactions in the capsomere of a murine polyomavirus (MPV) VLP. It is found that both low ionic strength and the intracapsomere disulfide bonds are favorable for maintaining a stable capsomere. Simulation results examining the effects of solution conditions on the stabilization of a capsomere were verified by calorimetry experiments. Simulation results of free energy decomposition indicate that hydrophobic interaction is favorable for the formation of a capsomere, whereas electrostatic interaction is unfavorable. With increasing ionic strength, the dominant interaction for the stabilization of a capsomere changes from hydrophobic to electrostatic. By comprehensive analyses, the key amino acid residues (hot spots) in VP1 protein aiding formation of a capsomere in different solution conditions have been identified. These results provide molecular insights into the stabilization of building blocks for VLP and are expected to have implications in their partitioning between the correct and off-pathway reactions in VLP assembly.

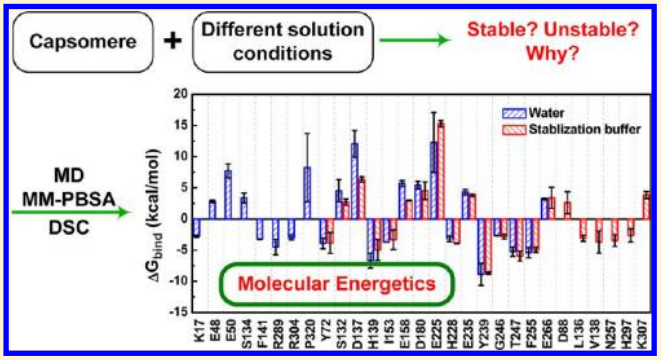

1. INTRODUCTION

Virus-like particles (VLPs) are highly organized nanoparticles that self-assemble from viral structural proteins. For example, murine polyomavirus (MPV) VLP is a capsid with 45 nm icosahedral (T = 7d) structure[1] formed by the self-assembly of the structural protein of MPV without the viral genetic material. The MPV VLP consists of 72 capsomeres comprising five VP1 molecules. VLP can mimic the organization and conformation of the authentic native virus but is noninfectious due to the lack of viral genetic material. Therefore, it has great potential in vaccinology, gene therapy, drug delivery, and materials science. Currently, VLP-based vaccines for hepatitis B virus (HBV)[2] and HPV[3,4] have been licensed commercially. However, the application of VLP is hindered by obstacles in their design and production due to low efficiency of self-assembly and difficulty in structural regulation.[5]

The assembly of viral structural proteins has been studied using both theoretical[6−8] and experimental[9−11] approaches. Recently, simulations of viruses using both coarse-grained and all-atom approaches have been exhaustively introduced.[12−14] Each VP1 monomer comprises a core β-barrel structure with a jelly roll topology, an amino-terminal extension, and a long carboxy-terminal arm. The C-terminal domain of each VP1 monomer "invades" a neighboring capsomere to form the principal intercapsomere contacts. These contacts can be strengthened by calcium ion chelation and disulfide bonding.[15,16] It has also been shown that the recombinant VP1 protein purified after expression in *E. coli* is isolated as a capsomere.[9] The purified capsomeres can associate to form capsid-like assemblies at high ionic strength. However, a variety of polymorphic aggregates of capsomeres are observed during in vitro self-assembly. The formation of aggregates (spherical or tubular particles) is dependent on experimental conditions such as pH, calcium ion concentration and ionic strength.[11,17] Besides these factors, the disulfide bonds are also considered important in assembly.[10,17] Though many efforts have been

Received: November 12, 2012
Revised: April 15, 2013
Published: April 15, 2013

focused on the structure as well as the formation of VLP,[10,18] understanding of the mechanism of VLP self-assembly is still far from fundamental. A recent study[19] suggests that aggregation of the capsomere subunit at the early assembly stage is highly detrimental to VLP formation, indicating the need for detailed and fundamental investigation into capsomere stabilization particularly under different physicochemical conditions.

In the present study, molecular dynamics (MD) simulations were performed and the molecular mechanics-Poisson−Boltzmann surface area (MM-PBSA) method was utilized to investigate the early stages of the viral assembly process and explore the molecular insight into the stabilization of a capsomere. MD simulation[20,21] is a powerful tool which can offer clear microscopic information with many successful applications.[22−30] Herein, various solution conditions with different ionic strengths have been considered in the MD simulations. The simulation results about the effect of solution conditions on the stabilization of a capsomere were validated by differential scanning calorimetry (DSC) experiments. The influence of the existence of disulfide bonds on the capsomere energy landscape has also been investigated. Moreover, the hot spots on VP1 for the formation of capsomere have been identified in different solution conditions.

2. MODELS AND METHODS

Model Construction. The all-atom (AA) model of the VP1 capsomere (Cap) was constructed based on the X-ray structure in Protein Data Bank (PDB ID: 1SID, http://www.rcsb.org/pdb/),[15] using the 5-fold symmetric part (pentamer). Residues from 17 to 320 were used according to recent experimental results.[18,31] The native conformation of Cap was shown in Figure S1. The total charge number carried in Cap was −15 (pH 7.0). Lysine and arginine were positively charged with a charge number of +1 each, while glutamic acid and aspartic acid were negatively charged with a charge number of −1 each. Five solution conditions for Cap (S1−S5) were considered (Table 1). The simple point charge (SPC) model was used for water molecule. Na^+ and Cl^- were considered as charged beads. For NH_4^+ and SO_4^{2-}, the topology was taken from the GROMOS96 43A1 force field. To construct the simulation box, the AA model of protein was first placed in the center of a cubic box ($12 \times 12 \times 12$ nm^3). Then, solvent molecules were placed randomly around the protein. Finally, the system was neutralized by adding Na^+ and Cl^- as counterions. The number of ions for each system as well as the number of water molecules was summarized in Table S1.

Table 1. Simulation Systems

system	protein	solution	SS bonds	remark
S1	Cap	water	−	water
S2	Cap	water	+	water with SS bonds
S3	Cap	200 mM NaCl	−	stabilization buffer
S4	Cap	0.5 M $(NH_4)_2SO_4$, 1 mM $CaCl_2$	+	assembly buffer
S5	Cap	1 M $(NH_4)_2SO_4$, 1 mM $CaCl_2$	+	aggregation buffer

Molecular Dynamics Simulations. MD simulations in the NPT ensemble were performed using GROMACS 4.5.3 package (http://www.gromacs.org/)[32,33] with the GROMOS96 43A1 force field.[34] Temperature was controlled at 298.15 K by the velocity-rescale (v-rescale) method[35] with a time constant of 0.5 ps. The pressure was controlled at 1 atm by the Berendsen barostat with coupling constants of 1.0 ps. Verlet algorithm was used with an integration time step of 2 fs. Linear Constraint Solver (LINCS) algorithm[36] was applied to constrain all bonds. Particle-mesh Ewald (PME) algorithm[37,38] was used to deal with the electrostatic interactions. The cutoffs of neighbor atom list, Coulomb potential, and Lennard-Jones (LJ) potential energies were all set to 0.9 nm. The initial velocities of particles were generated according to a Maxwell distribution at 298.15 K. Then, 5000 steps of steepest descent energy minimization were performed, followed by 500 ps equilibration with position restraints on the protein heavy atoms. The MD simulations were then performed for 20 ns.

Conformational and Molecular Interactions Analysis. The root-mean-square deviation (RMSD) from the crystal structure and potential energy of Cap were calculated using Gromacs.[32,33]

Electrostatics and Lipophilic Surface Potential. The electrostatic potential and lipophilic potential along the molecular surfaces of Cap were visualized using the MOLCAD program (Tripos, http://www.tripos.com/) from the SYBYL package.

Binding Free Energy Calculation. The binding free energy (ΔG_{bind}) between VP1 molecules of MPV capsomere was calculated using the MM-PBSA method[39] and the CHARMM[40] program (http://www.charmm-gui.org/). For all the simulation systems, 26 snapshots were extracted from the last 5 ns trajectory of each simulation performed by GROMACS at the interval of 200 ps. These snapshots in GROMACS format were converted into CHARMM format using our in-house scripts, and were further analyzed by the MM-PBSA method using the CHARMM program. ΔG_{bind} was calculated by eq 1.

$$\Delta G_{bind} = \langle \Delta G_{gas} \rangle + \langle \Delta G_{sol} \rangle - \langle T\Delta S \rangle \quad (1)$$

where the brackets, ⟨...⟩, indicate an average of an energy term along the MD simulation trajectory. $-T\Delta S$ is the entropic contribution. Herein, T is the temperature, and ΔS is the difference between the entropy of the complex and those of the isolated proteins; the relative free energy was analyzed without consideration of $-T\Delta S$. Moreover, the analysis concerned primarily per-residue electrostatic and hydrophobic contributions rather than the absolute binding free energy.

ΔG_{gas} contains an intermolecular electrostatic term (ΔG_{elec}), a van der Waals (vdW) term (ΔG_{vdW}), and an internal energy term (ΔG_{inter}). In this study, "the same trajectory method"[41] was used in all analyses. So, the internal energy term (ΔG_{inter}) is zero. Thus, ΔG_{gas} is the sum of ΔG_{elec} and ΔG_{vdW} [eq 2].

$$\Delta G_{gas} = \Delta G_{elec} + \Delta G_{vdW} \quad (2)$$

The solvation energy was divided into the electrostatic solvation energy (ΔG_{PB}) and the nonpolar solvation energy (ΔG_{np}) [eq 3].

$$\Delta G_{sol} = \Delta G_{PB} + \Delta G_{np} \quad (3)$$

where ΔG_{PB} was calculated by solving the linear Poisson−Boltzmann (PB) equation using the PBEQ module of the CHARMM program. The solute and solvent dielectric constants were set to 1 and 80, respectively. ΔG_{np}, which could be considered as the sum of a solvent−solvent cavity

dx.doi.org/10.1021/jp311170w | J. Phys. Chem. B 2013, 117, 5411−5421

term and a solute−solvent vdW term, was calculated according to eq 4.

$$G_{np} = \gamma \times \mathrm{SASA} + b \tag{4}$$

where the constants γ and b were set to 0.00542 kcal/(mol·Å^2) and 0.92 kcal/mol, respectively.[42] The solvent accessible surface area (SASA) was calculated using a water probe radius of 1.4 Å.

Free Energy Decomposition. The free energy contribution of each residue can be divided into polar (ΔG_{polar}) and nonpolar interactions ($\Delta G_{nonpolar}$) according to eq 5, and each part is the sum of two energy terms, as given in eqs 6 and 7. In the following analysis, ΔG_{polar} is considered as electrostatic interaction and $\Delta G_{nonpolar}$ as hydrophobic interaction.[43]

$$\Delta G_{bind} = \Delta G_{polar} + \Delta G_{nonpolar} \tag{5}$$

$$\Delta G_{polar} = \Delta G_{elec} + \Delta G_{PB} \tag{6}$$

$$\Delta G_{nonpolar} = \Delta G_{vdW} + \Delta G_{np} \tag{7}$$

where the electrostatic energy of each residue (ΔG_{polar}) is the sum of the intermolecular electrostatic energy (ΔG_{elec}) and the electrostatic solvation energy (ΔG_{PB}), as given in eq 6. The electrostatic contribution was decomposed by residues according to eq 8.

$$\Delta G^{j}_{elec} = \sum_{i\in \mathrm{capsomere}} \frac{1}{2} q_i \varphi_i^{\,j\in \mathrm{capsomere}} - \left[\sum_{i\in \mathrm{VP1}} \frac{1}{2} q_i \varphi_i^{\,j\in \mathrm{VP1}} + \sum_{i\in \mathrm{Rest}} \frac{1}{2} q_i \varphi_i^{\,j\in \mathrm{Rest}} \right] \tag{8}$$

The linear PB equation allows the decomposition of electrostatic solvation energy, since the electrostatic potential at point i (ϕ_i) can be calculated as the sum of the potentials created by other individual charges. The calculations were made on one VP1, whereas the other four VP1 molecules were considered as the counterpart [denoted by Rest in eq 8].

The vdW energy of each residue of VP1 was estimated as one-half of the vdW energy between itself and the others. The division by two ensures that the sum of individual contributions is equal to the total vdW energy of the capsomere. The nonpolar solvation energy of each residue is proportional to the loss in SASA of each residue and was calculated by eq 4.

Identification of Hot Spots. In the present study, both the residues making significant contributions to the binding free energy and the residues forming important intermolecular interactions to compensate the unfavorable solvation effect were considered as the hot spots. According to literature,[44] the hot spots were identified as those whose absolute value of free energy is larger than 2.5 kcal/mol. As shown in Figure S1, each VP1 has direct interaction with two neighboring VP1, leading to two binding interfaces. Herein, the two binding interfaces were labeled as A and B, respectively. In addition, because of the symmetric structure of the capsomere, calculations were performed on all five VP1 molecules, but only one VP1 was discussed to represent all five VP1 molecules. All energy values discussed below were the average values of five VP1 molecules.

DSC Analysis. To validate the MD simulation results, an assembly incompetent VP1 mutant lacking 63 C-terminal residues (VP1ΔC63; molar mass: 35.9 kDa; with a same sequence as the model used in the simulations) was expressed in *E. coli* and purified as previously described.[11] Purified VP1ΔC63 was dialyzed into stabilization buffer [40 mM tris, pH 8.0, 200 mM NaCl, 5 mM tris(2-carboxyethyl)phosphine (TCEP)], assembly buffer (40 mM tris, pH 8.0, 0.5 M $(NH_4)_2SO_4$, 1 mM $CaCl_2$) or aggregation buffer (40 mM Tris, pH 8.0, 1 M $(NH_4)_2SO_4$, 1 mM $CaCl_2$) and centrifuged at 22000 *g* and 4 °C for 15 min. The supernatant was extracted and the protein concentration was adjusted to 1 mg/mL based on UV−vis spectrophotometry [extinction coefficient, 1.5 L/(g cm)]. All buffers and samples were degassed using a MicroCal ThermoVac (GE Healthcare, NSW, Australia) prior to DSC experiments. DSC measurements were performed with a MicroCal VP-DSC microcalorimeter (GE Healthcare) with 0.497 mL reference and sample cells. Measurements were with a scan rate of 30 °C/h, from 25 to 90 °C, following standard manufacturer's instructions. Data were acquired with the VPVIEWER 2000 software (Version 1.4.27, MicroCal) and analyzed with The ORIGIN software (Version 7.0552, OriginLab Corporation, MA, USA). The data obtained were baseline subtracted and fitted with a nontwo-state model using the Levenberg−Marquardt nonlinear least-squares method, yielding the transition temperature (T_m) and the calorimetric enthalpy (ΔH_m).

The heat capacity change during the dissociation and unfolding reaction (ΔCp) was calculated from the initial and final baselines of the DSC thermogram extrapolated to T_m.[45] Using the experimentally calculated T_m, ΔH_m, and ΔCp, the difference in free energy between the capsomere and denatured states of VP1 ($\Delta G°$) as a function of T was calculated using eq 9.[46]

$$\Delta G°(T) = \Delta H_m\left(1 - \frac{T}{T_m}\right) + \Delta Cp\left[(T - T_m) - T \ln\left(\frac{T}{T_m}\right)\right] \tag{9}$$

3. RESULTS AND DISCUSSION

Electrostatics and Lipophilic Surface Potential. According to previous experimental studies,[17,47] electrostatic interaction is considered as an important issue for the stabilization of Cap. Therefore, the electrostatics surface potential is analyzed and presented in Figure 1. The exterior and interior surfaces of a Cap are colored according to the electrostatic potential. Heterogeneous charge distribution is observed. The exterior surface is predominantly neutral. Meanwhile, the interface between neighboring VP1 molecules is negative while the bottom of VP1 is positive. The portion of VP1 will form the interior of the capsid assembly, which can facilitate the loading of nucleic acid. Moreover, to examine the stabilization of Cap, the interior surface of Cap is presented in Figure 1d. Interestingly, the interior surface of a Cap is almost completely negatively charged. Simplistically, Cap would be expected to be unstable due to electrostatic repulsion between individual VP1 molecules.

Further analysis of lipophilic potential was performed to better understand the complex nature of Cap stabilization. In Figure 2, the exterior and interior surfaces of Cap are colored according to the lipophilic potential. It can be seen that the lipophilic potential surface is predominantly neutral. Meanwhile, hydrophobic patches are observed at the interface between neighboring VP1 molecules. It appears that hydrophobic interaction between individual VP1 molecules is the

dx.doi.org/10.1021/jp311170w | J. Phys. Chem. B 2013, 117, 5411−5421

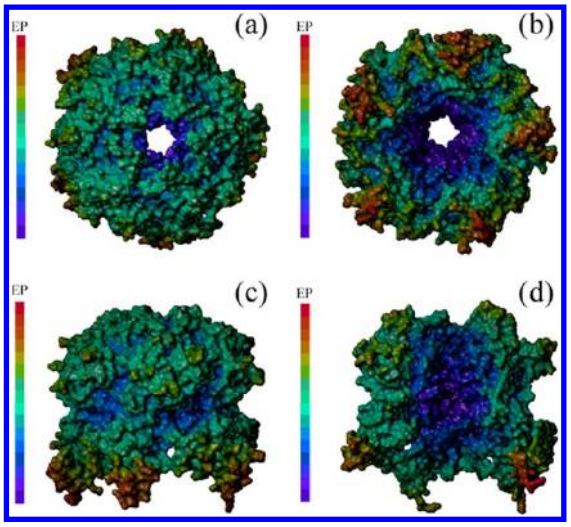

Figure 1. Exterior and interior surfaces of a Cap colored according to the electrostatic potential, where red is positive and purple is negative. (a) top view, (b) bottom view, and (c) side view of the exterior surface; (d) the interior surface. In panel d, only three of five VP1 monomers in Cap are displayed to reveal the interior surface. The crystal structure from PDB is used. The figures are prepared using the MOLCAD program (http://www.tripos.com/).

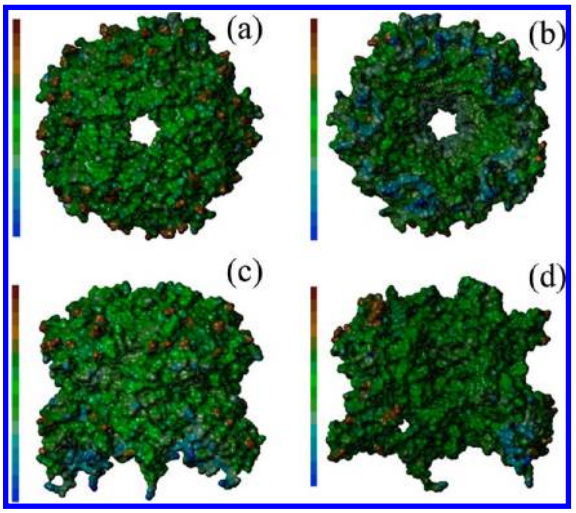

Figure 2. Exterior and interior surfaces of Cap colored according to the lipophilic potential, where brown is hydrophobic and blue is hydrophilic. (a) Top view, (b) bottom view, and (c) side view of the exterior surface; (d) the interior surface.

driving force for Cap stabilization, and competes favorably with electrostatic repulsion.

Binding Free Energy Analysis. To provide further insight into the stabilization of Cap and its implication to the self-assembly of VLP, the binding free energies within a Cap are evaluated using the MM-PBSA method. It has been proven by extensive studies that the relative binding free energy calculated by MM-PBSA coupled with MD simulations is able to reproduce the trend of affinities between protein molecules.[48,49] Herein, the efforts have been focused on the effect of solution conditions, using the same crystal structure as initial conformation in all simulations. It should be noted that only 20 ns simulation has been performed due to both the large simulation system and the limited computational resources. However, it can be seen from RMSD and potential energy that the Cap has been well equilibrated (Figure S2). So, the last 5 ns trajectory of each simulation has been used for the MM-PBSA analysis. In addition, due to its high computational demand and negligible change as compared with ΔG_{bind}, entropy contributions arising from changes in the degrees of freedom (translational, rotation, and vibration) of these proteins can be excluded in the free energy calculation in recent literatures.[39,50] Therefore, the binding free energy reported here is the relative binding free energy without consideration of the entropy. Herein, the effects of ionic strength and intracapsomere disulfide bond on the association between neighboring VP1 have been investigated using the relative binding free energy.

The binding free energies of Cap in different solutions are listed in Table 2. The lowest total binding free energy of Cap is observed in Stabilization Buffer (ΔG_{bind} = −445 kcal/mol, S3), whereas ΔG_{bind} for Cap in water (S1) is −303 kcal/mol, indicating that the presence of NaCl (200 mM) can lower the total binding free energy of Cap. In addition, ΔG_{bind} for Cap in water with disulfide bonds (S2) is −425 kcal/mol, indicating that intracapsomere disulfide bonding also stabilizes Cap. To evaluate the change caused by the deletion of N-terminal (residues from 1 to 16), a model including the N-termini (Cap-N) was constructed. Two solution conditions (S1 and S3) were considered (Table 1), and the binding free energies are evaluated using the MM-PBSA method. The results are shown in Table S2. A slight change of ΔG_{bind} from −445 kcal/mol to −443 kcal/mol in S3 is observed, while a change from −303 kcal/mol to −333 kcal/mol in S1 is observed. No significant change in total binding free energy is observed after the deletion of N-terminal. The AA model of Cap after the deletion of N-terminal was then used for the next discussion.

In the assembly buffer (S4), ΔG_{bind} of Cap is −346 kcal/mol, higher than that in stabilization buffer. In addition, a significant increase of ΔG_{bind} to −175 kcal/mol in aggregation buffer (S5) is observed, indicating a reduction of the structural stability of Cap in aggregation buffer. According to the experimental results in literature,[17] capsomeres associate into small regular shaped particles (VLPs) in assembly buffer, and into irregular aggregates in aggregation buffer. The MM-PBSA results

Table 2. Binding Free Energies (kcal/mol) of the Cap in Different Solution Conditions

system	ΔG_{vdW}	ΔG_{np}	ΔG_{elec}	ΔG_{PB}	$\Delta G_{nonpolar}$ [a]	ΔG_{polar} [b]	ΔG_{bind} [c]
S1	−692(61)	−176(3)	−3813(61)	4378(59)	−868(63)	565(20)	−303(59)
S2	−793(14)	−169(3)	−3441(89)	3978(62)	−962(11)	537(35)	−425(33)
S3	−801(27)	−178(2)	−3516(106)	4049(111)	−978(29)	533(16)	−445(39)
S4	−774(23)	−173(4)	−2831(130)	3431(117)	−947(22)	601(16)	−346(34)
S5	−681(55)	−176(1)	−2487(166)	3168(174)	−857(55)	682(33)	−175(23)

[a] $\Delta G_{nonpolar} = \Delta G_{vdW} + \Delta G_{np}$, hydrophobic interaction energy. [b] $\Delta G_{polar} = \Delta G_{elec} + \Delta G_{PB}$, electrostatic interaction energy. [c] $\Delta G_{bind} = \Delta G_{nonpolar} + \Delta G_{polar}$.

dx.doi.org/10.1021/jp311170w | J. Phys. Chem. B 2013, 117, 5411−5421

presented above provide possible rationale for these experimental observations from the viewpoint of binding free energy, suggesting that the formation of aggregates may be related to dissociation, which could favor undesirable intermolecular reaction due to exposure of hydrophobic residues. It is possible that capsomere structural stability considerations identified here augment more conventional considerations of colloidal stability, as identified for MPV capsomeres using measurements of the second virial coefficient,[11] to determine the final state of self-assembly or aggregation. It is widely accepted in the protein refolding literature that both structural and colloidal stability contribute to macromolecular organization and aggregation.[51]

To confirm the data obtained from the binding free energy analysis (Table 2), DSC was performed to ascertain the free energy of dissociation of assembly incompetent VP1ΔC63 capsomeres.[11] Figure 3 shows the DSC thermograms of

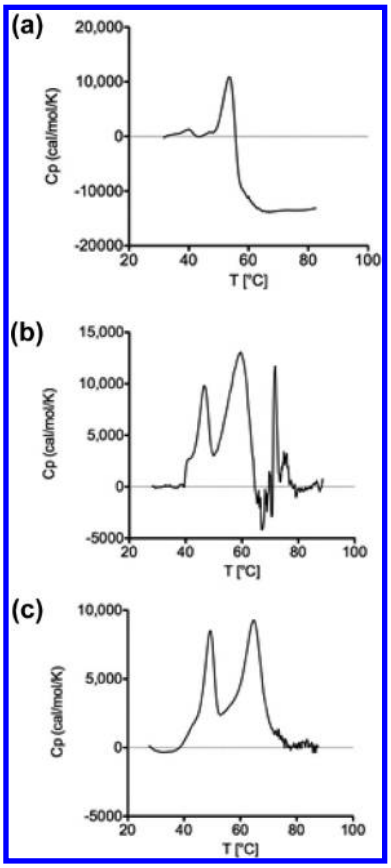

Figure 3. DSC results of VP1ΔC63 in (a) stabilization, (b) assembly, and (c) aggregation buffers.

VP1ΔC63 in Stabilization, assembly and disassembly buffers. In stabilization buffer (S3, Figure 3a), only a single endothermic event is observed in the temperature range of 50−56 °C, which corresponds well with the temperatures at which thermal denaturation of other capsid proteins occur.[52−54] The absence of other significant endotherms in the DSC thermogram suggests that the transitions for capsomere disassembly and unfolding of the VP1 monomer occur simultaneously[8] under this buffer condition. In contrast, two dominant endothermic events are observed in assembly (S4) and aggregation (S5) buffers (Figure 3b,c). The first endotherm is observed at approximately 50 °C while the second at approximately 60 °C. Such an observation indicates a dissociation/denaturation process wherein the capsomere (or assembled/aggregated capsomere) first dissociates and then unfolds.[54] Therefore, the first endotherm in assembly or aggregation buffers is used for the calculation of thermodynamic parameters associated with capsomere dissociation. Extraction of the same parameters for stabilization buffer was not feasible as the capsomere dissociation and protein denaturation events could not be adequately resolved.

The thermodynamic parameters calculated from the DSC thermograms are summarized in Table 3. The calculated ΔG° of dissociation at 25 °C for assembly and aggregation buffers are 23.8 ± 0.7 and 15.3 ± 2 kcal/mol, respectively. A higher ΔG° of dissociation indicates a larger energy barrier to capsomere dissociation, yielding a more stable capsomere. Therefore, these results agree with the relative free energy rankings by MD simulations (Table 2), indicating that the capsomere is more stable against dissociation in assembly buffer than in aggregation buffer.

Table 3. Thermodynamic Parameters from Calorimetric Scans of VP1ΔC63 in Different Solution Conditions

system	T_m (°C)	ΔH_m (kcal mol^{-1})	ΔCp (kcal mol^{-1} K^{-1})	ΔG° at 25 °C (kcal mol^{-1})
S4	46.31 ± 0.8	51.8 ± 2	0.21 ± 0.06	23.8 ± 0.7
S5	48.91 ± 0.2	31.3 ± 2	0.03 ± 0.01	15.3 ± 2

The free energy result was further decomposed to explore the molecular mechanism of the association between VP1 molecules, as shown in Table 2. It is found that the negative ΔG_{bind} is a sum of positive ΔG_{polar} and negative $\Delta G_{nonpolar}$ for both Cap and Ag-Cap in different solution conditions. It should be noted that the negative ΔG_{elec} is diminished by positive ΔG_{PB}. Therefore, nonpolar interaction is the main driving force for the binding of VP1 molecules. Moreover, it can be seen that almost 80% of the favorable nonpolar interaction is contributed by vdW interaction (ΔG_{vdW}) and the remaining 20% is contributed by nonpolar solvation terms (ΔG_{np}).

ΔG_{polar} of Cap in stabilization buffer is 533 kcal/mol, close to that in water (565 kcal/mol). However, $\Delta G_{nonpolar}$ of Cap in stabilization buffer is −978 kcal/mol, much lower than that in water (−868 kcal/mol). These results indicate that hydrophobic interaction is a dominant factor affecting the value of ΔG_{bind} of Cap at low ionic strength (0 and 0.2 M). However, in assembly buffer, similar $\Delta G_{nonpolar}$ (−947 kcal/mol) and higher ΔG_{polar} (601 kcal/mol) are observed as compared with the values in the control system (water-SS, S2). Moreover, in aggregation buffer, both higher $\Delta G_{nonpolar}$ and ΔG_{polar} are observed. The results suggest that the electrostatic energy becomes an important factor affecting ΔG_{bind} of Cap at high ionic strength (1.5 and 3.0 M). Therefore, hydrophobic interaction is the dominant factor at low ionic strength, while electrostatic interaction is the dominant factor at high ionic strength. It is proposed that this is the reason why VLP self-assembly is sensitive to ionic strength.

Free Energy Decomposition of Cap in Different Solutions. For further in-depth discussion, the binding free energy contribution of each residue within a Cap in stabilization buffer is compared with that in water (Figure 4). Eight key residues were identified in water but become insignificant in stabilization buffer, most of which are unfavorable for binding with very high ΔG_{bind}, e.g., E48 and P320. The sum of unfavorable binding free energy ($\Delta G_{bind,+}$) is

dx.doi.org/10.1021/jp311170w | J. Phys. Chem. B 2013, 117, 5411−5421

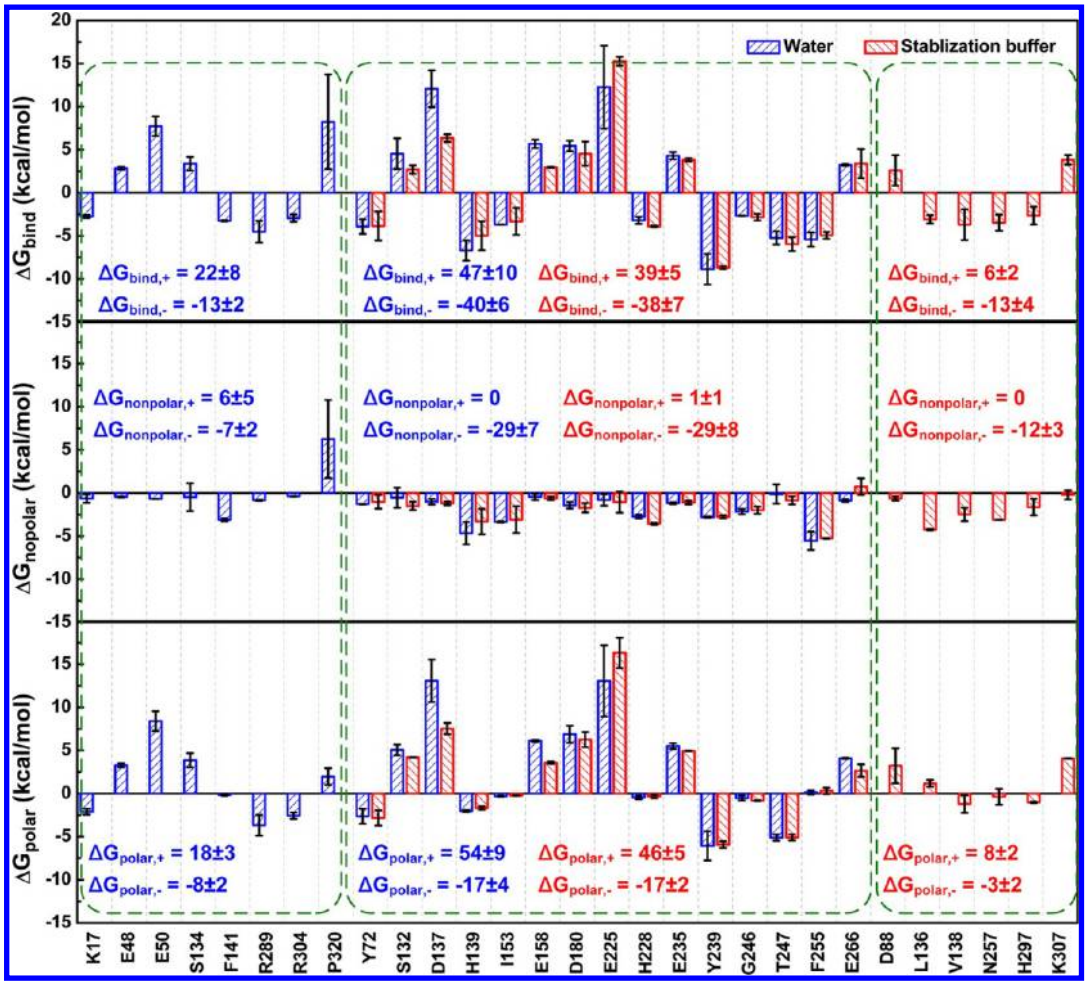

Figure 4. Binding free energy contribution of each residue within Cap in stabilization buffer as compared with that in water. Top panel, ΔG_{bind}; middle panel, $\Delta G_{nonpolar}$; bottom panel, ΔG_{polar}. For clarity, only the residues with the most favorable (<−2.5 kcal/mol) or unfavorable (>2.5 kcal/mol) contributions are shown. These residues are divided into three parts, i.e., residues only observed in water, residues observed in both water and stabilization buffer, and residues only observed in stabilization buffer. In each part, the residues are further divided into two clusters, including one favorable for binding and the other unfavorable for binding. The sum of the binding free energy in each cluster is calculated and provided in the figure.

Table 4. Changes of Free Energy Contributions of Key Residues in Different Solution Conditions

solution change	unfavorable H[a]	favorable H	unfavorable E[b]	favorable E	unfavorable contribution	favorable contribution	dominant factor
S1 to S3	↓[c]	↑	↓	↓	↓	–	H
S2 to S4	–	↓	↓	↓	↓	↓	H + E
S4 to S5	–	↑	↑	–	↑	↑	E

[a]Hydrophobic interaction. [b]Electrostatic interaction. [c]↑, ↓, and – represent enhancement, reduction, and no significant change, respectively. It should be noted that the enhancement is for the interaction rather than the algebraic value of the binding free energy. For example, the increase of favorable binding free energy indicates the reduction marked by ↓ as its algebraic value is negative.

22 kcal/mol, while that of favorable binding free energy ($\Delta G_{bind,-}$) is −13 kcal/mol. Meanwhile, six key residues are not observed in water but appear in stabilization buffer, most of which make favorable contributions for binding, e.g., L136, V138, N257, and H297, with a $\Delta G_{bind,+}$ of 6 kcal/mol and a $\Delta G_{bind,-}$ of −13 kcal/mol. Moreover, for the key residues observed in both the solution conditions, a significant decrease of $\Delta G_{bind,+}$ is observed in the stabilization buffer. So, it is clear that the unfavorable contribution for binding is diminished in the stabilization buffer, leading to a lower ΔG_{bind} (Table 2) and enhanced stabilization of Cap.

Furthermore, the free energy is decomposed into nonpolar and polar parts to respectively evaluate the contributions from hydrophobic and electrostatic interactions. It can be seen that the absolute value of $\Delta G_{nonpolar}$ of these key residues is smaller than that of ΔG_{polar} in both water and the stabilization buffer. However, $\Delta G_{nonpolar}$ is usually negative while ΔG_{polar} is usually positive, providing further evidence of the dominant role of hydrophobic interaction in binding at low ionic strength. Moreover, some key residues with high $\Delta G_{nonpolar,+}$ (e.g., P320) or high $\Delta G_{polar,+}$ (e.g., E50) in water disappear in the stabilization buffer. Instead, some residues appear with low $\Delta G_{nonpolar,-}$ (e.g., L136) and low $\Delta G_{polar,+}$ (e.g., D88), leading to improved binding. Moreover, it should be noted that larger decrease of $\Delta G_{nonpolar}$ is observed than that of ΔG_{polar}, confirming that the better binding in the stabilization buffer

dx.doi.org/10.1021/jp311170w | J. Phys. Chem. B 2013, 117, 5411−5421

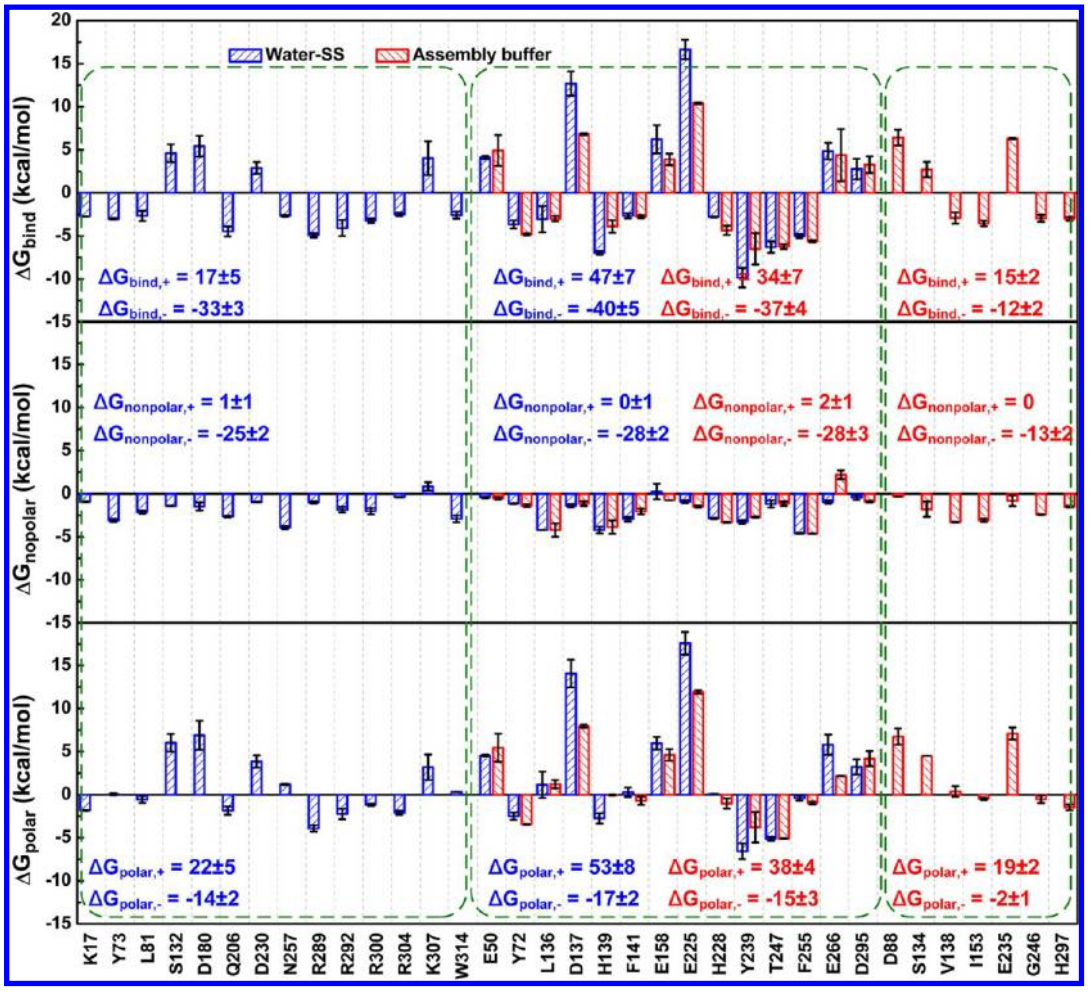

Figure 5. Binding free energy contribution of each residue within a Cap in assembly buffer as compared with that in water. Top panel, ΔG_{bind}; middle panel, $\Delta G_{nonpolar}$; bottom panel, ΔG_{polar}. Using the same protocol in Figure 4, the most important residues are selected and the sum of the binding free energies is calculated.

is mainly contributed by hydrophobic interaction. The contributions from each individual part and the changes induced by buffer switch are summarized in Table 4.

To evaluate the binding at high ionic strength, the free energy decomposition in the assembly and aggregation buffers were performed and compared to the results in the control condition (water-SS). As shown in Figure 5, 11 key residues are observed in both water and assembly buffer, including seven residues favorable and four residues unfavorable. Among these residues, a decrease of unfavorable contribution is observed, as indicated by the decrease of $\Delta G_{bind,+}$ from 47 to 34 kcal/mol. However, 10 residues with $\Delta G_{bind,-}$ of −33 kcal/mol in water disappear in assembly buffer, replaced by four residues with $\Delta G_{bind,-}$ of −12 kcal/mol, leading to an unfavorable contribution. This is the main reason for the increase of ΔG_{bind} in Table 2.

To evaluate the contributions from hydrophobic and electrostatic interactions, it is shown that both favorable nonpolar contribution ($\Delta G_{nonpolar,-}$) and favorable polar contribution ($\Delta G_{polar,-}$) are reduced in assembly buffer and the degree of reduction is similar, confirming that electrostatic interaction becomes more important at high ionic strength (Table 2). That is, from water to assembly buffer, both favorable hydrophobic and electrostatic interactions are reduced, leading to the more unstable (more active) state. The changes induced by buffer exchange are summarized in Table 4 in more details.

In aggregation buffer, as shown in Figure 6, an enhancement of favorable hydrophobic interaction is observed, as indicated by a decrease of $\Delta G_{nonpolar,-}$ from −4 (for the key residues observed in assembly buffer but not appearing in the aggregation buffer) to −10 kcal/mol (for the key residues not observed in assembly buffer but appearing in aggregation buffer). However, much larger enhancement of unfavorable electrostatic interaction is observed, as indicated by an increase of $\Delta G_{polar,+}$ from 6 to 21 kcal/mol. In the residues observed in both the solution conditions, similar $\Delta G_{nonpolar,+}$, $\Delta G_{nonpolar,-}$, and $\Delta G_{polar,-}$ are observed. However, a large increase of $\Delta G_{polar,+}$ is observed, leading to the increase of $\Delta G_{bind,+}$. The results further confirm that the electrostatic interaction becomes more important for the active state of Cap with increasing ionic strength (Table 2). That is, from assembly buffer to aggregation buffer, both favorable hydrophobic and unfavorable electrostatic interactions are enhanced and the latter is dominant, leading to the more unstable (more active) state (Table 4). The dominant factor is changed from hydrophobic interaction at low ionic strengths (S1 to S3) to electrostatic interaction at high ionic strengths (S4 to S5).

Identification of Hot Spots on Cap. The hot spots are identified based on the free energy decomposition results in

dx.doi.org/10.1021/jp311170w | J. Phys. Chem. B 2013, 117, 5411−5421

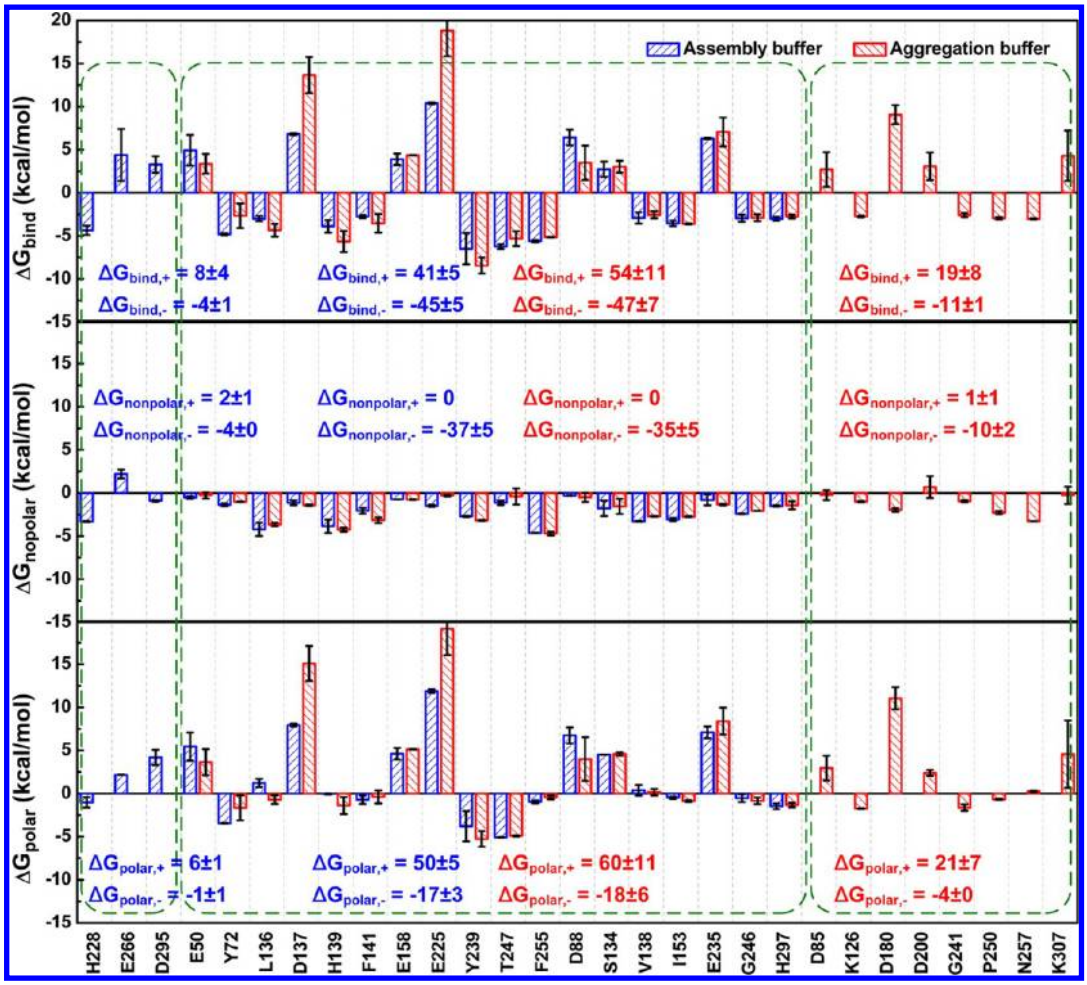

Figure 6. Binding free energy contribution of each residue within a Cap in aggregation buffer as compared with that in assembly buffer. Using the same protocol in Figure 4, the most important residues are selected and the sum of the binding free energy is calculated.

different solution conditions. Interfaces of a VP1 colored according to the free energy contribution of each residue are presented in Figure 7. For clarity, only the residues with the most favorable (<−2.5 kcal/mol) or unfavorable (>2.5 kcal/mol) contributions are labeled in the figure.

Twenty-three key residues with great contributions (Figure 7a) were identified, including 11 residues (D180, E225, H228, E235, Y239, G246, T247, E266, R289, R304, and P320) at interface A and 12 residues (K17, E48, E50, Y72, S132, S134, D137, H139, F141, I153, E158, and F255) at interface B. At interface A, six residues (H228, Y239, G246, T247, R289, and R304) are favorable while the other five residues (D180, E225, E235, E266, and P320) are unfavorable. At interface B, six residues (K17, Y72, H139, I153, F141, and F255) are favorable while the other six (E48, E50, S132, S134, D137, and E158) are unfavorable.

Once the solution condition is changed to Stabilization Buffer, 21 key residues with great contributions (Figure 7c) are observed, including 10 key residues (D88, D180, E225, H228, Y239, E235, G246, E266, T247, and H297) at interface A and 11 key residues (Y72, S132, L136, D137, V138, H139, I153, E158, F255, N257, and K307) at interface B. As compared with the interfaces in water, similar favorable patches are observed in both interfaces A and B in Stabilization Buffer. However, many unfavorable patches at interface B disappear, which is consistent with the results of free energy decomposition and provides more evidence in a direct manner.

In Assembly Buffer, 21 key residues with great contributions (Figure 7d) are observed, including 10 key residues (D88, E225, H228, E235, Y239, G246, T247, E266, D295, and H297) at interface A and 11 key residues (E50, Y72, S134, L136, D137, V138, H139, F141, I153, E158, and F255) at interface B. At interface A, five residues (H228, Y239, G246, T247, and H297) are favorable for binding while the other five (D88, E225, E235, E266, and D295) are unfavorable. At interface B, seven residues (Y72, L136, V138, H139, F141, I153, and F255) are favorable for binding while the other four (E50, S134, D137, and E158) are unfavorable. However, in the control system (water-SS), 29 key residues with great contributions (Figure 7b) are observed. It can be seen that in Assembly Buffer, less unfavorable patches are observed at interface B. However, less favorable patches are observed in both interfaces A and B, leading to a more active state (Tables 2 and 3).

When the solution condition is changed to Aggregation Buffer, 26 key residues with great contributions (Figure 7e) are observed, including 11 key residues (D85, D88, D180, D200, E225, E235, Y239, G241, G246, T247, and H297) at interface A and 15 key residues (E50, Y72, K126, S134, L136, D137, V138, H139, F141, I153, E158, P250, F255, N257, and K307) at interface B. At interface A, the unfavorable patches converge on the top, leading to an enhancement of repulsion between

dx.doi.org/10.1021/jp311170w | J. Phys. Chem. B 2013, 117, 5411−5421

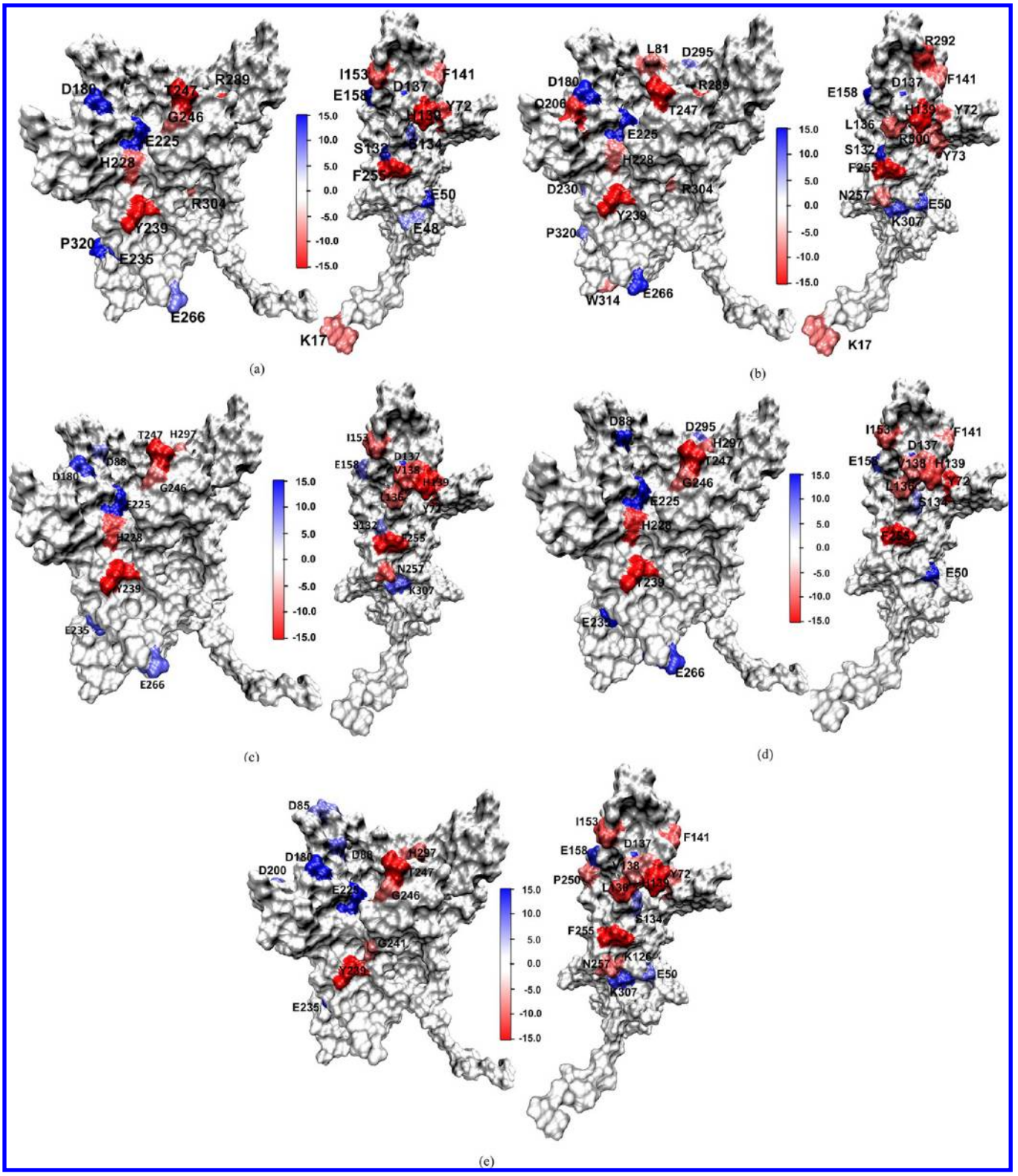

Figure 7. Interfaces of VP1 colored according to the free energy contribution of each residue, including interface A (left) and interface B (right). Solution conditions: (a) water; (b) water with SS bonds; (c) stabilization buffer; (d) assembly buffer; (e) and aggregation buffer. For clarity, only the residues with the most favorable (<−2.5 kcal/mol) or unfavorable (>2.5 kcal/mol) contributions are labeled. Binding free energy ranges from red (most negative) to blue (most positive). The figures are prepared using the visual molecular dynamics (VMD) software (http://www.ks.uiuc.edu/Research/vmd/).

VP1 molecules. Moreover, at interface B, more unfavorable patches and more favorable patches are both observed. However, the increase of unfavorable patches is dominant, leading to a more active state (Tables 2 and 3).

dx.doi.org/10.1021/jp311170w | J. Phys. Chem. B 2013, 117, 5411−5421

4. CONCLUSIONS

MD simulations coupled with MM-PBSA analysis are adopted to examine the molecular interactions within a Cap of MPV VLP, and to explore the molecular basis involved in VLP self-assembly at the Cap level. It is shown that both low ionic strength and intracapsomere disulfide bonds are favorable for maintaining a stable Cap. Changes in free energy due to changes in solution conditions will be critically important during VLP assembly, where a fine balance of structural and colloidal stability is required to assemble an authentic VLP and avoid the formation of off-pathway aggregates.[19] The simulation results concerning the relative impacts of solution conditions on the stabilization of a capsomere have been verified by DSC experiments. Furthermore, from the results of free energy decomposition, it can be seen that hydrophobic interaction is the main driving force for the formation of Cap at low ionic strength. However, with increasing ionic strength, electrostatic interaction becomes more important. Therefore, in aggregation buffer having high ionic strength, electrostatic interaction becomes the dominant factor. The variation of hot spots on VP1 under different solution conditions is consistent with the free energy decomposition and further confirms simulation results emphasizing the impacts of solution conditions, in a direct manner. Therefore, this work has provided molecular insights into the molecular mechanisms of VP1-VP1 association, in a way that may prove helpful for the design of new VP1 mutants that benefit VLP assembly.

■ ASSOCIATED CONTENT

Ⓢ Supporting Information

Conformation of Cap. This material is available free of charge via the Internet at http://pubs.acs.org.

■ AUTHOR INFORMATION

Corresponding Author

*Tel & Fax: +86 22 27404981. E-mail: ysun@tju.edu.cn.

Notes

The authors declare no competing financial interest.

■ ACKNOWLEDGMENTS

This work was supported by the Natural Science Foundation of China (Nos. 21236005 and 21006069), the Key Technologies R&D Program of International Cooperation of Tianjin, China, the Innovation Foundation of Tianjin University, and Queensland Government's "National and International Research Alliances" Program. Experimental constructs were initially generated using funding provided by the Australian Research Council (Federation Fellowship to APJM) and the Queensland Smart Futures Fund (Premier's Fellowship to APJM). We are thankful to the Advanced Instrumental Detection & Analytical Center, School of Chemical Engineering and Technology, Tianjin University for providing access to the SYBYL 6.92 software package.

■ REFERENCES

(1) Stehle, T.; Yan, Y.; Benjamin, T. L.; Harrison, S. C. *Nature* **1994**, *369*, 160−163.
(2) McAleer, W. J.; Buynak, E. B.; Maigetter, R. Z.; Wampler, D. E.; Miller, W. J.; Hilleman, M. R. *Nature* **1984**, *307*, 178−180.
(3) Koutsky, L. A.; Ault, K. A.; Wheeler, C. M.; Brown, D. R.; Barr, E.; Alvarez, F. B.; Chiacchierini, L. M.; Jansen, K. U. *New Engl. J. Med.* **2002**, *347*, 1645−1651.
(4) Villa, L. L.; Costa, R.; Petta, C. A.; Andrade, R. P.; Paavonen, J.; Iversen, O. E.; Olsson, S. E.; Hoye, J.; Steinwall, M.; Riis-Johannessen, G.; et al. *Br. J. Cancer* **2006**, *95*, 1459−1466.
(5) Pattenden, L. K.; Middelberg, A.; Niebert, M.; Lipin, D. I. *Trends Biotechnol.* **2005**, *23*, 523−529.
(6) Schwartz, R.; Shor, P. W.; Prevelige, P. E., Jr; Berger, B. *Biophys. J.* **1998**, *75*, 2626−2636.
(7) Zlotnick, A. *J. Mol. Recognit.* **2005**, *18*, 479−490.
(8) Katen, S.; Zlotnick, A. *Method. Enzymol.* **2009**, *455*, 395−417.
(9) Salunke, D. M.; Caspar, D. L. D.; Garcea, R. L. *Cell* **1986**, *46*, 895−904.
(10) Schmidt, U.; Rudolph, R.; Bohm, G. *J. Virol.* **2000**, *74*, 1658−1662.
(11) Chuan, Y. P.; Fan, Y. Y.; Lua, L.; Middelberg, A. *J. R. Soc. Interface* **2010**, *7*, 409−421.
(12) Joshi, H.; Singharoy, A.; Sereda, Y. V.; Cheluvaraja, S. C.; Ortoleva, P. J. *Prog. Biophys. Mol. Biol.* **2011**, *107*, 200−217.
(13) Nguyen, H. D.; Reddy, V. S.; Brooks, C. L. *J. Am. Chem. Soc.* **2009**, *131*, 2606−2614.
(14) Hagan, M. F.; Elrad, O. M.; Jack, R. L. *J. Chem. Phys.* **2011**, *135*, 104115−13.
(15) Stehle, T.; Harrison, S. C. *Structure* **1996**, *4*, 183−194.
(16) Stehle, T.; Harrison, S. C. *EMBO J.* **1997**, *16*, 5139−5148.
(17) Salunke, D. M.; Caspar, D. L.; Garcea, R. L. *Biophys. J.* **1989**, *56*, 887−900.
(18) Middelberg, A.; Rivera-Hernandez, T.; Wibowo, N.; Lua, L.; Fan, Y. Y.; Magor, G.; Chang, C.; Chuan, Y. P.; Good, M. F.; Batzloff, M. R. *Vaccine* **2011**, *29*, 7154−7162.
(19) Ding, Y.; Chuan, Y. P.; He, L.; Middelberg, A. P. *Biotechnol. Bioeng.* **2010**, *107*, 550−560.
(20) Karplus, M.; McCammon, J. A. *Nat. Struct. Biol.* **2002**, *9*, 646−652.
(21) Daggett, V. *Chem. Rev.* **2006**, *106*, 1898−1916.
(22) Zheng, J.; Jang, H.; Ma, B.; Nussinov, R. *J. Phys. Chem. B* **2008**, *112*, 6856−6865.
(23) Zheng, J.; Yu, X.; Wang, J.; Yang, J.; Wang, Q. *J. Phys. Chem. B* **2010**, *114*, 463−470.
(24) Straub, J. E.; Thirumalai, D. *Curr. Opin. Struct. Biol.* **2010**, *20*, 187−195.
(25) Sgourakis, N. G.; Merced-Serrano, M.; Boutsidis, C.; Drineas, P.; Du, Z.; Wang, C.; Garcia, A. E. *J. Mol. Biol.* **2011**, *405*, 570−583.
(26) Buchete, N. V.; Tycko, R.; Hummer, G. *J. Mol. Biol.* **2005**, *353*, 804−821.
(27) de, P. M.; de, M. G.; Serrano, L.; Colombo, G. *J. Mol. Biol.* **2005**, *349*, 583−596.
(28) Takeda, T.; Klimov, D. K. *J. Mol. Biol.* **2007**, *368*, 1202−1213.
(29) Tarus, B.; Straub, J. E.; Thirumalai, D. *J. Mol. Biol.* **2008**, *379*, 815−829.
(30) Gsponer, J.; Ferrara, P.; Caflisch, A. *J. Mol. Graph. Modell.* **2001**, *20*, 169−182.
(31) Wibowo, N.; Chuan, Y. P.; Lua, L. H. L.; Middelberg, A. P. J. *Chem. Eng. Sci.* **2012**, DOI: 10.1016/j.ces.2012.04.001.
(32) Berendsen, H. J.; Vanderspoel, D.; Vandrunen, R. *Comput. Phys. Commun.* **1995**, *91*, 43−56.
(33) Lindahl, E.; Hess, B.; van, S. D. *J. Mol. Model.* **2001**, *7*, 306−317.
(34) Mackerell, A. D. *J. Comput. Chem.* **2004**, *25*, 1584−1604.
(35) Bussi, G.; Donadio, D.; Parrinello, M. *J. Chem. Phys.* **2007**, 126.
(36) Hess, B.; Bekker, H.; Berendsen, H. J. C.; Fraaije, J. G. E. M. *J. Comput. Chem.* **1997**, *18*, 1463−1472.
(37) Darden, T.; York, D.; Pedersen, L. *J. Chem. Phys.* **1993**, *98*, 10089−10092.
(38) Essmann, U.; Perera, L.; Berkowitz, M. L.; Darden, T.; Lee, H.; Pedersen, L. G. *J. Chem. Phys.* **1995**, *103*, 8577−8593.
(39) Huang, B.; Liu, F. F.; Dong, X. Y.; Sun, Y. *J. Phys. Chem. B* **2011**, *115*, 4168−4176.
(40) Brooks, B. R.; Brooks, C. L.; Mackerell, A. D.; Nilsson, L.; Petrella, R. J.; Roux, B.; Won, Y.; Archontis, G.; Bartels, C.; Boresch, S.; et al. *J. Comput. Chem.* **2009**, *30*, 1545−1614.
(41) Zoete, V.; Meuwly, M.; Karplus, M. *Proteins* **2005**, *61*, 79−93.

(42) Gorfe, A. A.; Jelesarov, I. *Biochemistry* **2003**, *42*, 11568−11576.
(43) Li, J.; Zhang, L.; Sun, Y. *J. Mol. Graph. Model.* **2012**, *37*, 49−58.
(44) Lafont, V.; Schaefer, M.; Stote, R. H.; Altschuh, D.; Dejaegere, A. *Proteins* **2007**, *67*, 418−434.
(45) Richardson, M. J.; Savill, N. G. *Polymer* **1977**, *18*, 413−414.
(46) Bruylants, G.; Wouters, J.; Michaux, C. *Curr. Med. Chem.* **2005**, *12*, 2011−2020.
(47) Brady, J. N.; Consigli, R. A. *J. Virol.* **1978**, *27*, 436−442.
(48) Yan, C. L.; Kaoud, T.; Lee, S. B.; Dalby, K. N.; Ren, P. Y. *J. Phys. Chem. B* **2011**, *115*, 1491−1502.
(49) Muzzioli, E.; Del Rio, A.; Rastelli, G. *Chem. Biol. Drug Des.* **2011**, *78*, 252−259.
(50) Joshi, M.; Ebalunode, J. O.; Briggs, J. M. *Proteins* **2009**, *75*, 323−335.
(51) Chi, E. Y.; Krishnan, S.; Kendrick, B. S.; Chang, B. S.; Carpenter, J. F.; Randolph, T. W. *Protein Sci.* **2003**, *12*, 903−913.
(52) Ross, P. D.; Conway, J. F.; Cheng, N. Q.; Dierkes, L.; Firek, B. A.; Hendrix, R. W.; Steven, A. C.; Duda, R. L. *J. Mol. Biol.* **2006**, *364*, 512−525.
(53) Galisteo, M. L.; Gordon, C. L.; King, J. *J. Biol. Chem.* **1995**, *270*, 16595−16601.
(54) Deschuyteneer, M.; Elouahabi, A.; Plainchamp, D.; Plisnier, M.; Soete, D.; Corazza, Y.; Lockman, L.; Giannini, S.; Deschamps, M. *Human Vaccines* **2010**, *6*, 407−419.